

Gradual development of S-shaped gears

Gorazd Hlebanja^{1,*}

¹University of Novo mesto, Na Loko 2, 8000 Novo mesto, Slovenia

Abstract. Search for an improved gear tooth flank shape arose from heavy industry problems rolling mills. Original involute gears suffered severe flank damages. So, better gear teeth flanks should improve contact circumstances, decrease the flank pressure, and enhance a lubrication film. This was achieved by a curved, pole symmetric path of contact by purely graphical methods. And the developed gears, proven in heavy industry applications, showed highly improved properties. Specimens of both gear geometries, which were made of tempered and nitrided alloy steel, were tested on an FZG testing machine, and results confirmed the theoretical foundations of S-gears. Then it was necessary to replace the graphical method by a numerical one and to define the tool. So, the rack profile was defined by a pole symmetric parabolic-type function, which in turn defined the path of contact and finally gears with an arbitrary number of teeth. Many applications were developed with S-gear shape, e.g., helical, crossed, and planetary gears, various worm drives, etc. S-gear concept was also used with polymer gears and high transmission ratio planetary gears. Lately, this concept was used to develop crossed helical gear drive with perpendicular shafts. Such drives are often used in centrifuge drives (e. g. Alfa-Laval) and this implementation with the module $m = 5$ mm uses a large driving gear with 60 teeth (with the left-handed helix angle of 30°) on the horizontal shaft and a smaller driven gear with 20 teeth (with the right-handed helix angle of 60°) on the vertical shaft.

This paper is a tribute to work of Professor Jože Hlebanja (1926-2022) whose research was dedicated to gears with improved properties, namely S-gears.

1 Introduction

Involute gears transmit power through convex–convex contact. This type of gears is prevalingly used in today industry. This can be attributed to the brilliant Euler’s invention and their gradual development over centuries and improvements in both manufacturing technologies and materials. However, the intrinsic property of the involute gear is its curvature radius function in the dedendum part when approaching the base circle. Values in this area are small in general and limited to zero approaching the base circle. This implies high contact loads in this area. Additionally, for gears with a low number of teeth, the dedendum flank is comparatively very short, thus invoking excessive sliding and friction losses and the possibility of premature damage. Yet another problem is undercutting of the dedendum area. Therefore, there exists a permanent need for improved gears, with such features as a convex-concave contact, a stronger root, improved curvature radii, better lubrication conditions, etc.

2 Gears for rolling mills

Several hot and cold rolling mills in former Yugoslavia during 70ties with arrangements powered by drives from 110 up to 1500 kW reported problems with roller gears

and severe wear of their teeth flanks. So, it was decided to use gears with improved characteristics. Several variants of tooth flank shapes were designed, produced, and tested for various applications in several ironworks. Finally, the tooth flank shape based on curved path of contact with the nonzero initial pressure angle as illustrated in Fig. 1 prevailed.

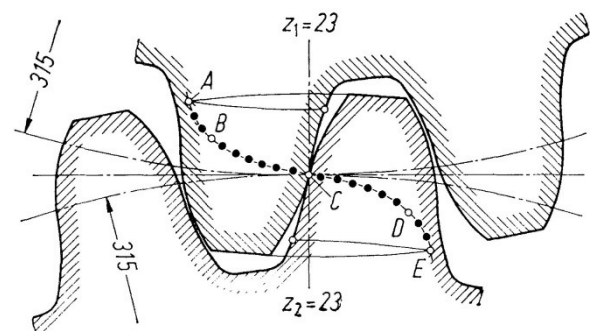


Fig. 1. Industrial implementation of gears with the curved path of contact [1,2].

The path of contact is a sequence of contact points of the meshing gear pair transmitting rotation. Each contact point complies with the law of gearing. The path of contact should also warrant sufficiently high contact ratio. The contact load in the kinematic pole C depends on the

* Corresponding author: gorazd.hlebanja@siol.net

initial pressure angle α_C . The starting pressure angle α_A is constrained due to the contact ratio and contact load. Gears of the same module with an arbitrary number of teeth can be manufactured by the same tool profile when the path of contact is pole-symmetric.

Gears are designed according to the root strength and the flank durability. The path of contact shape and the root fillet influence the root thickness, whereas the flank shape essentially influences its durability. The basic factors influencing flank durability are the reduced radii of curvature and amount of sliding. Higher radii imply lower Hertzian pressure. The sliding circumstances are essentially improved in the case of convex-concave contact. The research showed that areas of the path of contact with a higher curvature imply lower sliding and higher reduced radii of curvature.

Inworks Sisak installed gears represented in Fig.1 in their heavy-duty rolling mill line, since the former involute gears suffered severe scuffing in gear teeth dedendum and addendum areas soon after installation. The line was powered by a 1500 kW electric motor with 80 to 160 RPM and furthermore reduced by 2. So, the rolling mill gears rotated with 40 to 80 RPM. The herringbone gear pair was made of alloy steel 30CrMoV9. Gears had $z=23$, $d=630$ mm, and helix angle $\beta=28,274^\circ$. S-formed gearing was an essential improvement, operating for several decades.

3 Experiments with S- and E-gears

Further research was orientated to define the S-gear path of contact in such a way to ensure smaller flank pressure, better lubrication and less sliding. Additionally, the pressure angle in the vicinity of the kinematic pole C should be very similar as in the involute case. Fig. 2 represents such a pole symmetric path of contact, with gradually increasing curvature towards the meshing start and end. The corresponding rack profile is designated by a and the gear tooth flank by b. The maximal coordinates of the meshing start and end points, A and E depend on the maximal pressure angle and the contact ratio.

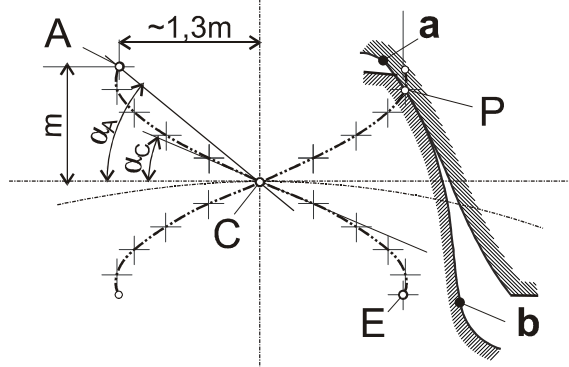


Fig. 2. Path of contact with gradually increasing curvature [3,4]

Next, S- and E-gears were compared by experiments conducted on an FZG testing machine. Both gear types were examined to discover endurance (a) against pitting

of teeth flanks, (b) scuffing of teeth flanks, and (c) surface heating, wear, and efficiency.

The selected material was alloy steel 42CrMo4, which was heat treated to 28-30 HRC prior to toothing. Experimental lots comprised (a) hardened and tempered gears, and (b) hardened, tempered, and plasma nitrided gears. Technical data of the gears are collected in Table 1. Meshing gears (pinion and gear) are illustrated in Fig.3.

Table 1: Technical data of experimental gears [5,6].

Symbol	Description	S-gears		E-gears	
		Pinion	Wheel	Pinion	Wheel
m [mm]	Module	4,575		4,5	
Z	Number of teeth	16	24	16	24
x	Profile shift	-	-	+0,233	+0,12
d [mm]	Pitch diameter	73,2	109,8	73,2	109,8
α_w [°]	Pressure angle	20° 22°		22,438°	
b [mm]	Face width	20		20	
a [mm]	Centre distance	91,5		91,5	
n [r/min]	Rotational speed	2100	1400	2100	1400
v_t [m/s]	Pitch line velocity	8,048		8,048	
Pitch deviation according to DIN 3962					
f_p	Single	7-8		7	
F_p	Cumulative	7-8		7	

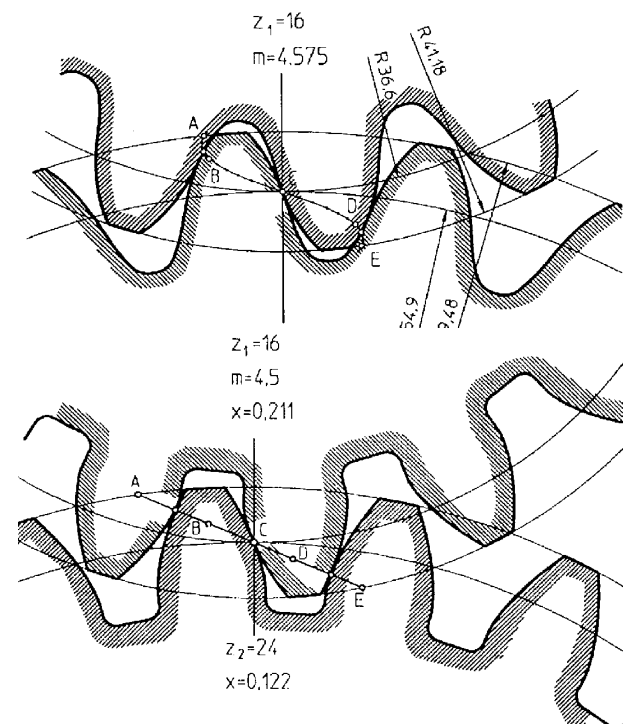


Fig. 3. Meshing pinion ($z=16$) and gear ($z=24$): (a) S-gear pair (above), and (b) E-gear pair (below) [4].

Regarding endurance against root fracture, the measure of such endurance is the tooth root stress depending on the tooth root thickness and fillet radius. In this case (see Fig. 3) S-gear teeth are stronger in the root and their fillet radius is larger, so they are less prone to fracture (app. 20%) [5].

In general, we use the Hertzian contact pressure [7] as a measure of tooth-flank load as regards pitting damage, which is calculated for cylindrical gear pairs by the following equation:

$$\sigma_H = 0,418 \sqrt{\frac{w_{bn} \cdot E'}{\rho_{red}}} \quad (1)$$

The contact pressure along the path of contact was calculated for both gear types and for the input load of $T_1 = 302$ Nm on the pinion (gears made of steel) and presented in Fig. 4. The highest value of σ_H is in the kinematic pole C. After that it decreases towards B and D. Since the contact becomes convex-concave near meshing start and end areas, that is near A and E, for the S-gears, the reduced radii of curvature become longer and σ_H becomes apparently small, which is advantageous for S-gears.

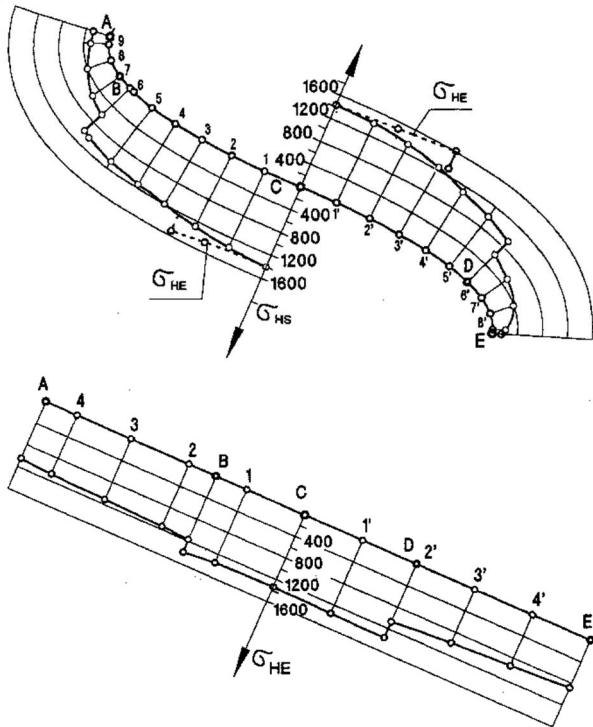


Fig. 4. Hertzian pressure along the path of contact for (a) S-gear pair (above), and (b) E-gear pair (below) [5,6,8].

So, the gear flanks of both gear types are equally loaded in a region of pitch diameter. The pressure in C is the highest for S-gears, whereas E-gears have maximal values in B and D, so, the probability of pitting damage is higher there. E-gears exhibit pitting mostly in the vicinity of the single mesh point B in the zone of negative sliding. Experiments showed that S-gears exhibit pitting always within the range of the operating diameter of a gear.

Another important measure of endurance against damages of tooth flanks is oil film thickness h_0 , which is defined by the Dowson-Higginson's equation [9]. This, experimentally based equation implies that h_0 is highly influenced by oil properties and sum of contact velocities u , moderately influenced by geometry (ρ_{red}), and less influenced by load and material properties. So, for the same operating conditions S-gears exhibit higher relative velocities which contribute to a thicker oil film. This is illustrated for the meshing start circumstances in Fig. 5.

Oil temperature and mass temperature of gears were kept constant, whereas lubricant was replaced regularly by the same brand and type. Under these conditions the

Blok's flash temperature equation [10] can be used as a measure of tooth-flank load regarding scuffing damage.

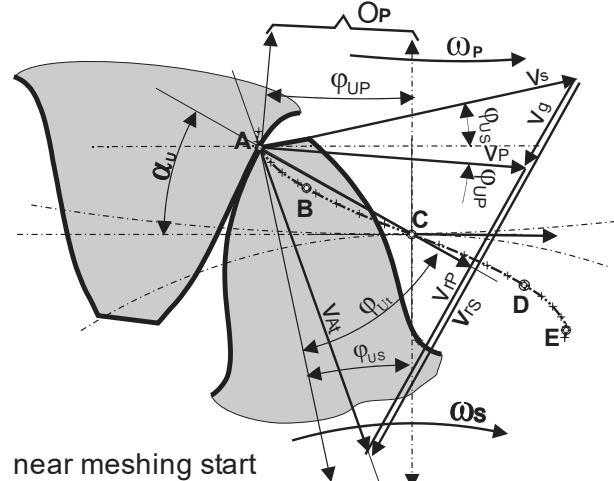


Fig. 5. Velocities in the vicinity of the meshing start $u = v_{rP} + v_{tS}$ [8]

The flash temperature increment is zero in the kinematic pole, then it rises sharply towards B and E. In the case of S-gears the temperature rise has a maximum between B and C and drops towards B. And temperatures between A and B (also D and E) are apparently lower. Whereas the values for E-gears are maximal in A. So, the E-gears develop unfavourable flash temperature conditions compared to the S-gears.

The flash temperatures for S-gears are in general smaller, especially at the meshing start. This is due to higher radii of curvature ρ_{red} , higher relative velocities and the smaller coefficient of friction μ . Fig. 5 shows v_{rP} and v_{tS} as the velocities in tangential direction to the tooth profile in the contact point P. In the case of curved path of contact the relative velocities are than that of a hypothetical E-gear with the path of contact through the same point P. This means that rolling component in the contact point is prevailing over sliding. Therefore, the flash temperature and coefficient of friction are lower and oil-film thicker. Therefore, wear and energy loss are smaller.

S-N curves (Wöhler) curves were plotted based on FZG experiments to individually evaluate lifetime based on (a) pitting damages, and (b) scuffing. The experiments were conducted according to DIN 51354 [5,6,8].

It was stated that S-gears with $\alpha_{wt} = 22^\circ$ achieved to some extent higher (pitting) durability of tooth-flanks against pitting in comparison to S-gears with $\alpha_{wt} = 20^\circ$ and E-gears with $\alpha_{wt} = 22,438^\circ$.

The risk of scuffing damage is smaller for S-gears, which was proven through experimenting on the FZG rig. E-gears developed first scuffing damage on the load level 11 ($w_{tb} = 615$ N/mm). In the case of S-gears there was no damage even after load level 12.

The oil temperature was monitored during the FZG testing and it was demonstrated that the temperature increase of oil against pinion torque was in favor of S-gears [8]. E.g., the measured temperature for the torque of 534 Nm on pinion was 118 °C for S-gears and 127 °C for E-gears.

Wear of S- and E-gears was estimated by weighting of samples before and after achieved 4×10^6 cycles on the FZG testing machine. Wear of S-gears was between $\frac{1}{3}$ and $\frac{1}{2}$ of that in E-gears [5].

4 Further development

The previously described properties initiated further development of helical, crossed and planetary gears and also ZS worm drive based on S-gear path of contact [11], which is illustrated in Fig. 6.

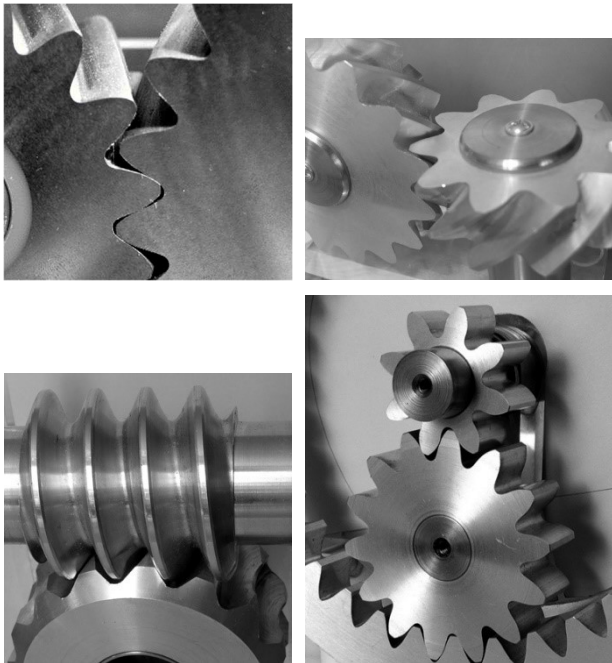


Fig. 6. Working models for various S-type gearings: (a) helical; (b) crossed helical; (c) ZS worm drive; (d) planetary arrangement [11]

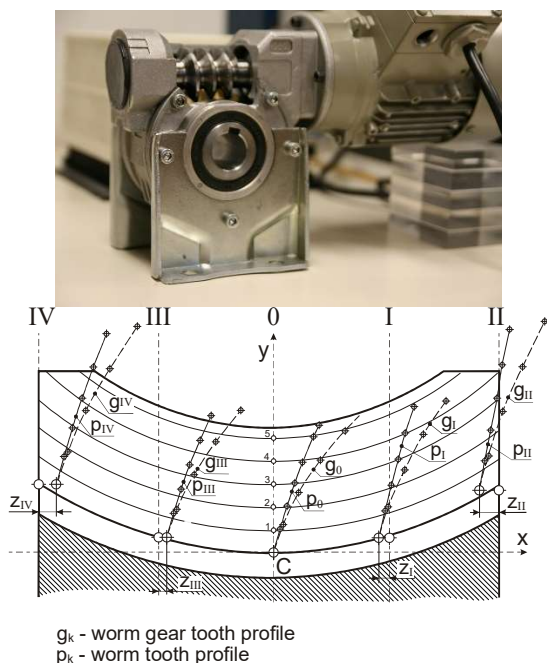


Fig. 7. Parabolic worm-gear in the industrial housing (above) worm and worm gear profiles in parallel planes (below) [12]

A cylindrical worm-gearing with a progressively curved shape of teeth flanks, the so-called parabolic worm gear drives [12] is illustrated in Fig. 7. The proposed approach is based on the mathematically defined worm tooth profile in the worm axial plane, wherefrom the worm gear tooth profile derives and profiles in any parallel plane can be calculated, and teeth flanks are defined. The primary feature of the proposed teeth flanks is their progressive curvature and continual concave-convex contact. Worm and worm gear meshing of such an arrangement generates better lubricating oil film, resulting in better EHD lubrication conditions, therefore reduced energy losses and lower wear damages are anticipated. An experimental worm-gearing loaded under working conditions verified theoretical considerations. Computer simulation also confirmed contact theory of the proposed gearing. Additionally, the worm gear was installed in the industrial housing, where an observation window was cut off.

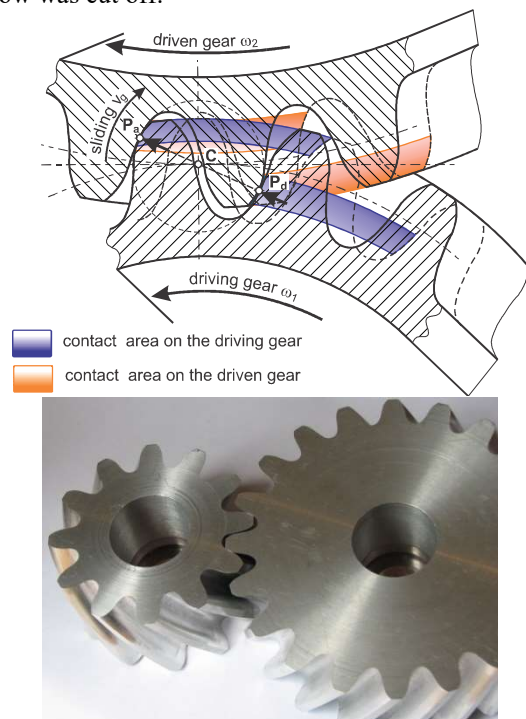


Fig. 8. UPT gear pair contact areas (above) UPT gear pair with $m_n=5$ mm; $z_1=12$, $z_2=20$ (below) [13]

Uniform power transmission (UPT) gears [13] illustrated in Fig. 8 are characterised by the tooth flank profile comprised of three circular arcs, with the first arc forming the addendum; the second forming the dedendum; the third arc forming the intermediate section, which prevents the flanks from touching as they rotate around the kinematic pole C. The advantage of this solution is a simple flank geometry, which is easier in terms of tools, while the relative rotation of one gear vis-à-vis its pair is similar to the movement of the shaft in the bearing. The essential element of the UPT gears is the absence of a pitch line and the gear-teeth contact in the transverse plane. In addition, there is no sliding between the teeth flanks in the transverse plane. Power is mainly transmitted by the rolling of the teeth flanks at both contact points, with the simultaneous sliding of the teeth flanks around

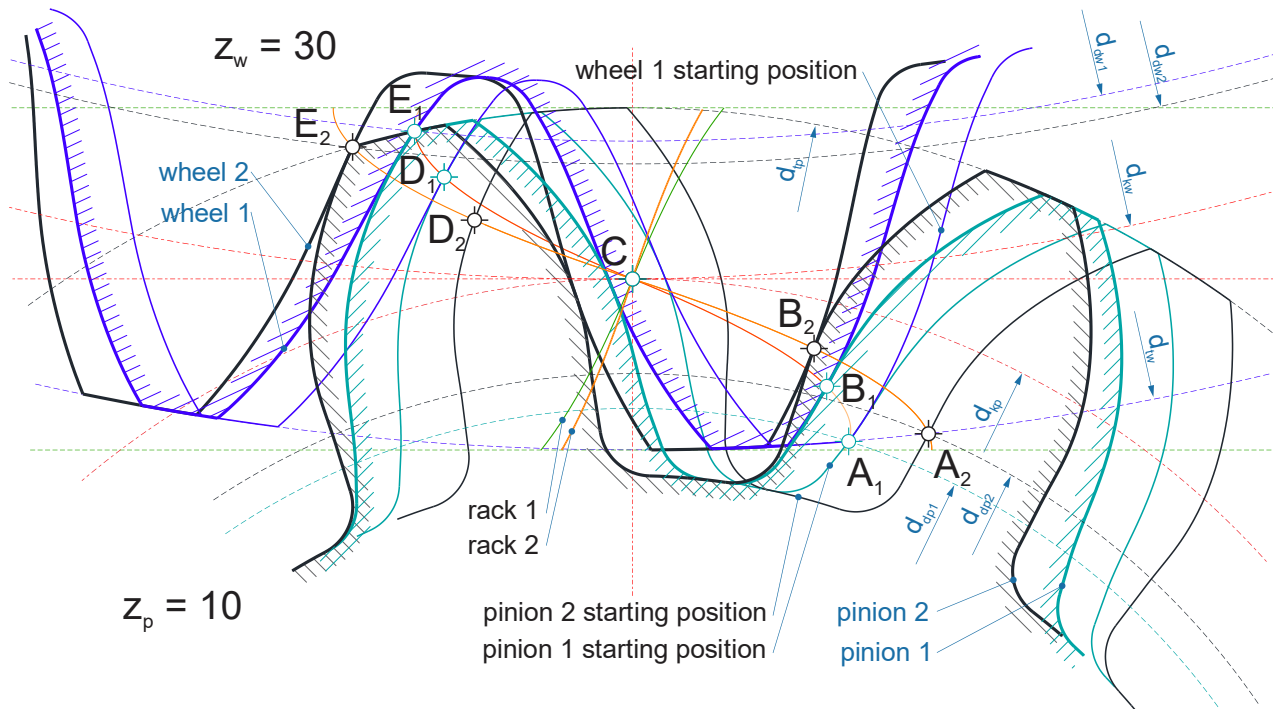


Fig. 9. External gear pairs with pinion $z_p=10$ and wheel $z_w=30$. The generating rack 1 with (initial) pressure angle $\alpha_w=22^\circ$ and rack 2 with $\alpha_w 18^\circ$ (pinion 1- petrol green, wheel 1 - blue; pinion 2 and wheel 2 black) [15]

the pitch point C. The contact load is divided to two contact points. Better lubrication conditions can be expected because of the thicker oil-film thickness and lower heat generation. And the most important features of the UPT gears are non-intermittent sliding and power transmission. These features indicate that UPT gears can be applied with heavy loads in non-stop operating condition, for example, in the power transmission of wind turbines, gear units for refinery services, and similar applications.

5 Mathematical definition of the rack profile

A basic requirement when defining gear tooth flank geometry is that a rack tooth flank as well as a driving and a driven gear flank imply the same path of contact and that they follow the law of gearing. So, instead of defining a curved path of contact (with some already described features) one can define an appropriate rack profile and, in this context a cutting tool. Eq. 2 [14] defines the upper part of the generating rack profile, whereas its lower part is pole symmetric.

$$y_{p_i} = a_p(1 - (1 - x_{p_i})^n) \quad (2)$$

where (x_{p_i}, y_{p_i}) are Cartesian coordinates originating in the kinematic pole C, the a_p parameter designates the size factor and n is the exponent. The defined rack profile defines a single path of contact from which gears of an arbitrary number of teeth derive. In order to define the path of contact it is necessary that the above function is differentiable. Regarding a_p and n , these parameters serve as tooth form factors. They should be optimized in such a way that the produced gears conform to the anticipated

requirements. E.g., gears with initial pressure angle $\alpha_{w0}=22^\circ$ are strong in the root, whereas increasing α_{w0} even further gives even stronger root but at the same time this induces a bigger contact force and reversely lower α_{w0} means lower contact force and thinner root. The situation is illustrated in Fig. 9 for mating pinion ($z=10$) and wheel ($z=30$).

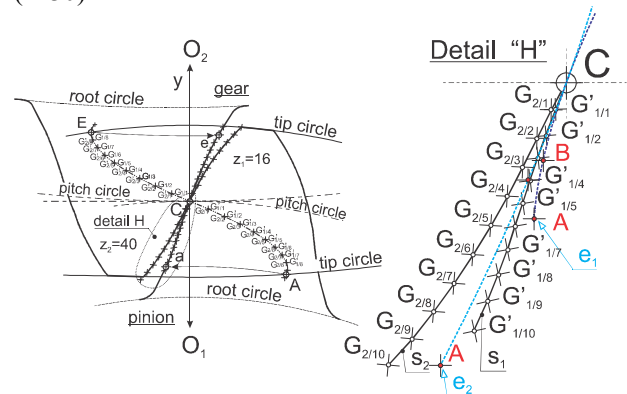


Fig. 10. Contact density – the length of sliding of the wheel addendum on the pinion dedendum [16]

Another important characteristic of S-gears is the amount of sliding. The mating gear teeth flanks combine the pinion dedendum and the gear addendum flanks from the meshing start to the kinematic pole C and the pinion addendum and the gear dedendum from C towards the meshing end point. The contact is propagating on the path of contact by rolling and sliding. The active size of the pinion dedendum is smaller than that of the gear addendum, as shown in Fig.10. This implies amount of sliding of the addendum on the shorter pinion dedendum, which is illustrated in Fig. 10 for S-gears. The amount of sliding also implies thermal impact. In general, the

dedendum-addendum size difference depends on module, number of teeth, pressure angle. For S-gears the said difference also depends on forming factors – the height and the exponent. The size difference in the case of S-gears is comparatively more convenient, so less sliding is produced along the contact propagation compared to the involute case. Fig. 10 (detail) also shows the dedendum and the corresponding addendum of the E-gear. The starting pressure angle for the S-gears is 22° and that of the E-gears 20° . The contacting addendum flank length of the latter is about twice as large as that of the pinion. This also implies that S-gears produce less frictional power than E-gears [16].

6 Plastic gears

Gears made of technical polymers became inevitable in many industries, also for demanding applications. So, the question arose: How would S-gears made of plastic behave?

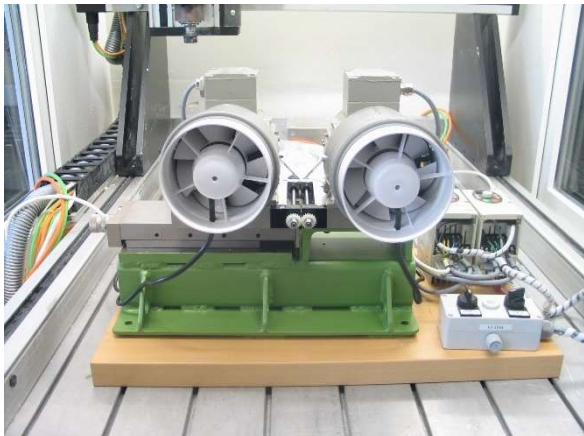


Fig. 11. Front view of the testing rig for small plastic gears [17]



Fig. 12. Front view of the testing rig for small plastic gears [17]

A special testing rig was built in LECAD (FME, University of Ljubljana) to examine small plastic gears with the module $m=1$ mm and $z=20$, Fig. 11. Since the temperature behaviour of polymer gears in operation is important, the testing system was designed to enable observation of both gears in action by a fast thermal camera. The apparatus consists of two shortcut asynchronous motors powered by frequency inverters, which enable speed control, and sliding precisely. The aim of this testing rig is to deliver Wöhler curves for each

material and geometry combination of gears. Regarding materials, mostly POM – PA6 combination is used, due to good frictional behaviour. Steel – polymer combinations are also of importance.

Fig. 12 reveals injection moulded S-gears ($\alpha_{w0}=27^\circ$, $n=1.4$) vs. the involute gears of the same size ($m=1$ mm, $z_1=z_2=20$). The difference is obvious, but it can be also observed that the axis distance in the case of S-gears does not correspond to that of the involute gears. It is already agreed that S-gears can mate even with deviated axis distance [18], but efficiency of such action has not been defined precisely, yet. This implies that the design of moulds should be carried out with a consideration of actual shrinkage of materials, which is not an easy task. Another consideration is that the quality of moulded gears is rather low and how does it influence the precise flank geometry, particularly in the case of S-gears.

Later, raw cylinders were injection moulded and then cut to final dimensions and teeth dimensions adapted for thermal expansion [15].

This type of testing rigs was upgraded by Podkrižnik co. and used to deliver S-N curves for gears made from materials of interest, Fig. 13 [15].

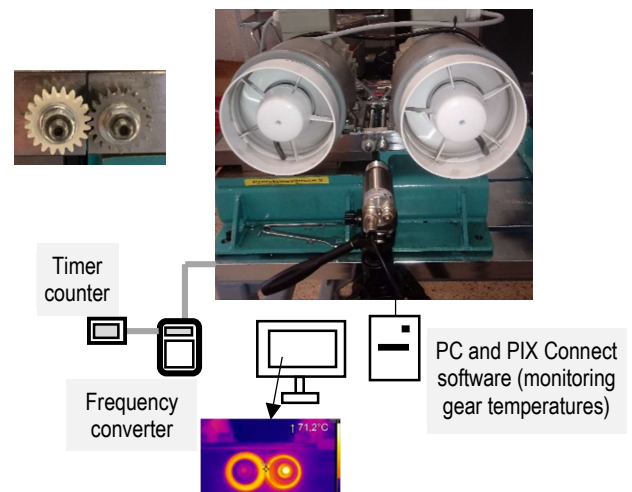


Fig. 13. Upgraded testing rig for lifetime testing of thermo-plastic gears with thermal camera to monitor temperature data [15]

Steel pinion and POM wheel combination was used to compare S- and E- gears. Gear geometry is already known, apart from the initial pressure angle (18°) of S-gears. Rather high torque sequence was selected (1,5 Nm, 1,3 Nm, and 1,1 Nm to reduce the time necessary for completed S-N curves) Tests were run at 1400 RPM.

E-profiles achieved apparently lower number of cycles up to collapse than S-gears for all torques. Thermal behaviour in the contact is shown in Fig. 14 for 1,5 Nm and 1400 RPM.

The temperature-time dependency consists of three main sections, namely: a) running-in area where thermoplastic driven gear fits to steel gear in terms of tooth flanks; b) a phase of a quasi-stationary operating at app. stable temperature; c) a phase of increasing gear wear that, in combination with fatigue causes failure of thermoplastic gears.

The running-in phase of the E- gear pair exhibits a transient phenomenon with the increased temperature in the contact. This can be attributed to the unmodified involute tooth tip profile, the high load, and subsequent teeth deformation, the phenomenon which was also reported in [7], p. 98. The driven gear suffers an additional impact at a meshing start point A and the temperature rise. The consequence is rather high initial wear of a driven plastic gear. S-gears do not exhibit such effects, so the temperature rise proceeds without initial maximum until the second, stationary phase.

In the next phase, relatively stationary conditions prevail. For E gears the initially high temperature drops and prevails until the final phase. Uniform wear occurs in this phase for both gear types. The last phase of the lifetime test shows significant changes of the gears. This is due to the increased wear above the critical limit in connection with the fatigue of the material, which causes degradation of the bonds between the molecules in the material and the subsequent teeth failure.

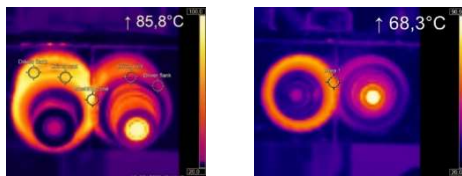


Fig. 14. Comparison of E- and S-gearing with the steel pinion and POM wheel at $M = 1.5 \text{ Nm}$ and $n = 1400 \text{ min}^{-1}$
 a.) temperature spot in the meshing area E (left) and S (right) gear. b.) temperature-time profiles (S – green, E – grey) [15]

Research of polymer gears is progressing with various material combinations and investigation of wear development [19].

7 Helical gear pairs with perpendicular shafts

Characteristic of S-gears is the convex-concave contact near contact start and end. The dedendum flank is always concave and the tooth tip convex. The model shown in Fig. 15 shows that helical gears can adopt S-form and working crossed helical S-gears can be produced [20].

The path of contact on each tooth flank surface can be regarded as a union of contact point of both teeth flanks. The situation for the driven gear is illustrated in Fig. 16. The tooth flanks of both gears are helical and contain the

convex and the concave part. Power transmission always follows over surfaces with the opposite curvature sign.

A tooth flank contact always occurs on a pair of helices, which determines the first main contact plane. This fact is valid for E- and S-gears. The second main contact plane is determined by the path of contact, which means that the contact and kinematic conditions can be uniformly determined.



Fig. 15. Model of a crossed helical gear with a progressively curved path of contact, $\beta = 45^\circ$

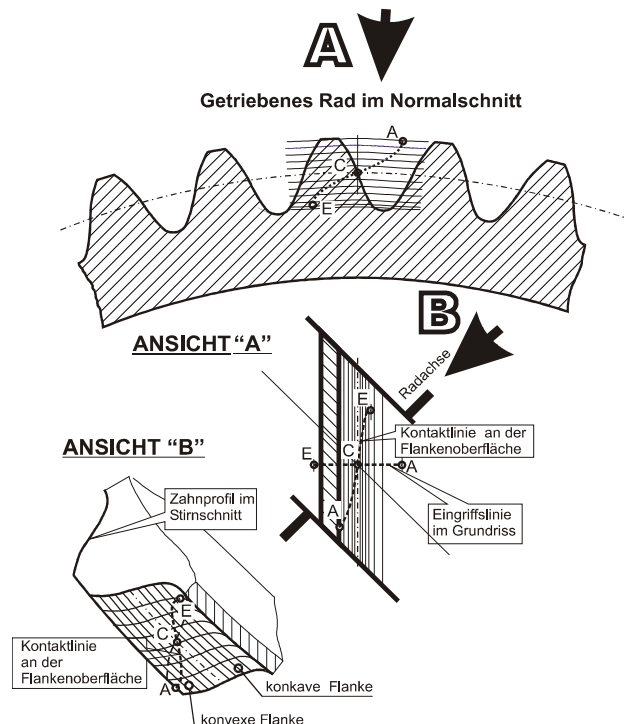


Fig. 16. Path of contact on the tooth flank of the driven gear

Yet, another application is a crossed helical gear drive based on S-gear concepts for centrifuge drives. This gear drive consists of two cylindrical gears with helical teeth fitted to perpendicular shafts. They are often used in cream separation drives (e. g. Alfa-Laval). This implementation uses a large driving gear with 60 teeth on the horizontal shaft and a smaller driven gear with 20 teeth on the vertical shaft. The module of the gear mechanism is $m = 5 \text{ mm}$, the angle of left-hand helix angle on the

large driving gear is $\beta_1 = 30^\circ$, and the right-hand helix angle on the small driven gear is $\beta_2 = 60^\circ$. The working model is presented in Fig. 17.



Fig. 17. Working model of the crossed helical S-gear drive

8 Conclusion

This paper is an attempt to illuminate the gradual development of the S-gear concept from the start with gearing problems in heavy industry, gears based on the curved path of contact, mathematical definition of the rack profile – a cutting tool, and later applications. Gears made of polymers seem to be an important application. The centrifuge drive was the last application developed by Prof. J.-Hlebanja, recently.

Some applications are researched and developed in industry. This refers to polymer gears and high ratio intelligent gear drives. However, numerous research questions regarding S-gearings are still unsolved and at the same time there are numerous possible applications improving current state of the art.

References

1. J. Hlebanja, Konkav-konvexe Verzahnung Ermittlung der Zahnflanken und einige Grenzfälle, *Antriebstechnik* **15** (1976) 6
2. J. Hlebanja, Betriebserfahrung an Kammwalzgetrieben mit Sonderverzahnungen, *VDI-Berichte* Nr. 332, (1979), p. 283-288
3. J. Hlebanja, Influence of the Path of Contact Shape on Sliding Condition between Tooth Flanks; MPT' 91 JSME Int. Conf., Hiroshima 1991
4. J. Hlebanja, Gesetzmöglichkeiten bei der Bildung neuer Sonderverzahnungen. *Antriebstechnik*. **32** (1993), Nr. 4, p. 110-112
5. G. Hlebanja, J. Hlebanja, I. Okorn, Research of gears with progressive path of contact. DETC2000/PTG-14384, ASME International (2000), 7 p.
6. J. Hlebanja, I. Okorn Charakteristische Eigenschaften von Zahnradern mit stetig gekrümmter Eingriffslinie, *Antriebstechnik* **38** (1999), Nr.12
7. G. Niemann, H. Winter. *Maschinenelemente*, Band II, 2. Auflage. Springer Verlag (1989)
8. G. Hlebanja, J. Hlebanja, Contribution to the development of cylindrical gears, 4. Int. Conf. BAPT, Springer, (2013), p. 309-320
9. D. Dowson, G.R. Higginson, *Elasto-Hydrodynamic Lubrication*. SI Edition. Pergamon Press (1977)
10. F.H. Theyse, Die Blitztemperatur Hypothese nach Blok und ihre praktische Anwendungen bei Zahnradern. *Schmiertechnik* **14** (1967), Heft 1, p. 22-29
11. J. Hlebanja, G. Hlebanja, Anwendbarkeit der S-Verzahnung im Getriebebau: Nichtevoventische Verzahnungen weiterentwickelt. *Antriebstechnik*, **44** (2005) Nr. 2, p. 34-38.
12. G. Hlebanja, J. Hlebanja, M. Čarman, Cylindrical worm gearings with progressively curved shape of teeth flanks. *Journal of Mech. Eng.*, (2009) **55** No. 1, p. 5-14
13. G. Hlebanja, J. Hlebanja, Uniform power transmission gears. *Journal of Mech. Eng.*, (2009) **55** No. 7/8, p. 472-483.
14. J. Hlebanja, G. Hlebanja, Spur gears with a curved path of contact for small gearing dimensions VDI-Berichte 2108 (2010) p. 1281-1294
15. G. Hlebanja, M. Erjavec, M. Hriberšek, L. Knez, S. Kulovec, Theory and applications based on S-gear geometry; in S.P. Radzevich (Ed.), *Recent advances in gearing: scientific theory and applications*, 1st ed. Springer Nature, (2022), p. 51-87
16. G. Hlebanja, S. Kulovec, D. Zorko, J. Hlebanja, J. Duhovnik, Influence of the tooth flank shape on thermal load of the gear, (2017) VDI-Berichte, 2294.2, p. 1583-1592
17. G. Hlebanja, S. Kulovec, J. Hlebanja, J. Duhovnik, S-gears made of polymers. *Ventil*, No. 5 (2014) **20**, p. 358-367
18. G. Hlebanja, J., Hlebanja, Influence of axis distance variation on rotation transmission in S-gears: example on heavy duty gears, *VDI-Berichte*, 2199, (2013) p. 669-679.
19. M. Hriberšek, M. Erjavec, G. Hlebanja, S. Kulovec, Durability testing and characterization of POM gears. *Eng. failure analysis*. Jun. (2021), **124**, p. 1-11
20. J. Hlebanja, G. Hlebanja, M. Umberger, S-gear design rules. *Ventil*, No. 4, (2020) **26**, p. 254-263